On the Characterization of the Local Structure in Liquid Water by Various Order Parameters. Supporting Information

Elise Duboué-Dijon and Damien Laage*

École Normale Supérieure-PSL Research University, Département de Chimie, Sorbonne Universités - UPMC Univ Paris 06, CNRS UMR 8640 PASTEUR, 24, rue Lhomond, 75005 Paris, France

E-mail: damien.laage@ens.fr

*To whom correspondence should be addressed

Complementary analysis of the correlation between order parameters in bulk water

Two dimensional probability density distributions. Figure S1 shows the two-dimensional probability density distributions of water local structure in the bulk at 298 K for pairs of order parameters that are not already represented in Fig. 1 of the parent manuscript. The corresponding Pearson correlation coefficients are given in Table 1.

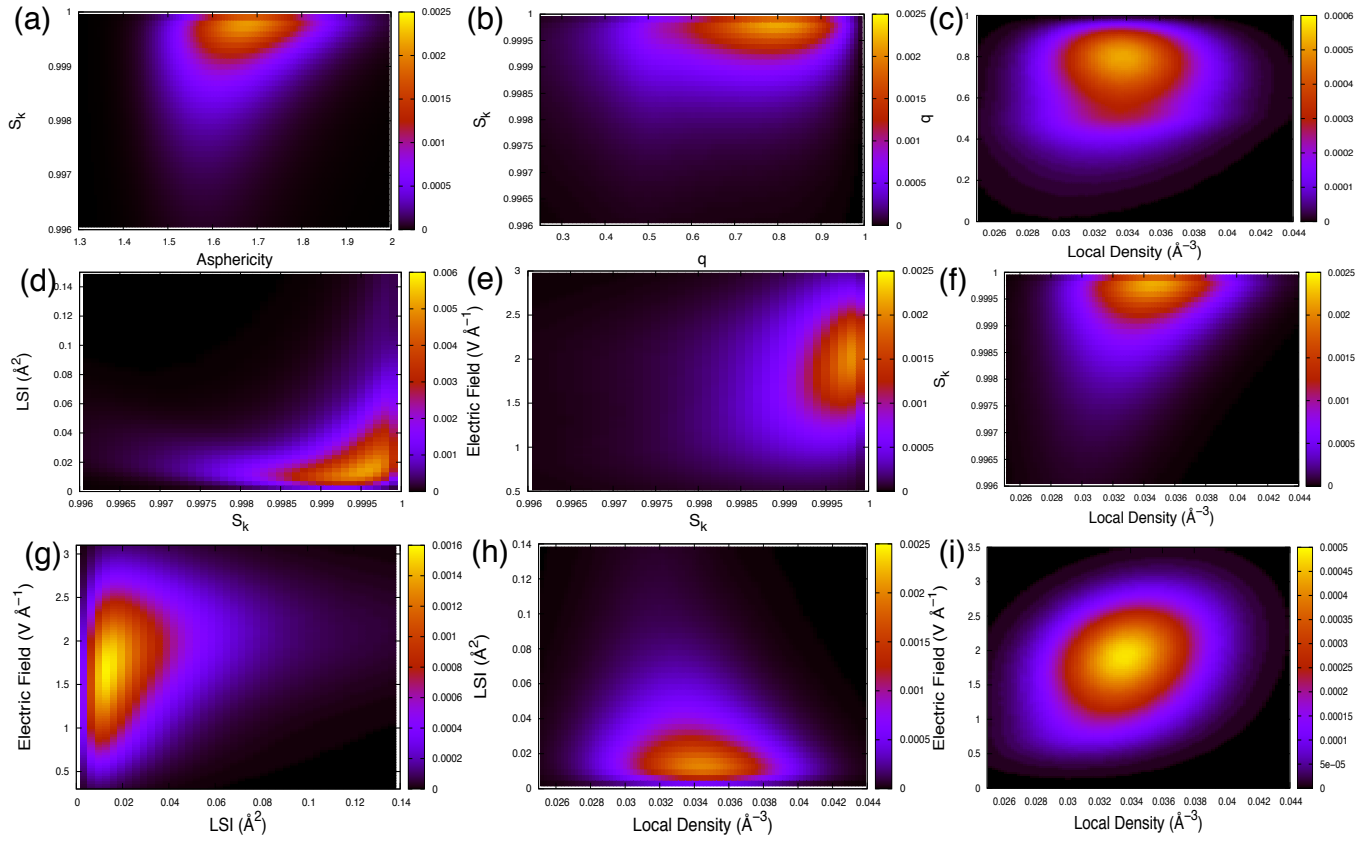

Figure S1: Two-dimensional probability density distributions of water local structures in the bulk at 298 K for selected pairs of order parameters

"Off-diagonal" structures. We now determine the features of structures which are reported as ordered by one parameter but as disordered according to an other parameter, i.e. structures which appear in off-diagonal locations in the two-dimensional probability distributions in Figs. 1 and S1.

We first focus on the q and η order parameters and we consider three sub-ensembles of configurations, respectively (high q, high η), (high q, low η) and (low q, low η) (Table S1). For each such subset of configurations, we compute the average LSI and S_k, together with the number $n_{\text{coor3.7A}^\circ}$ of water neighbors within 3.7 Å, which are involved in the LSI definition (see Eq. 3), and compare these values with their averages over all configurations (Table S1). Our results first show that (high q, high η) configurations also have high LSI and S_k values and can thus be unequivocally classified as "ordered". The same considerations apply to the (low q, low η) systems. In contrast, in (high q, low η) configurations, we find a large decrease in the LSI and a strong increase in the coordination number with respect to the bulk average. These structures are therefore angularly ordered (leading to a high q), but radially disordered, with additional neighbors in the second shell, as shown by the disorder reported by the other parameters. The apparent inconsistency between the order parameters is therefore due to the different types of disorder which are probed.

Table S1: Average relative shifts in η, q, LSI and S_k with respect to their 298 K bulk averages (in %) for all water neighbors within 3.7 Å and for a series of different configuration subensembles defined by the range of η and q values.

	High η - high q $\eta > 1.75$ & $q > 0.8$	Low η - high q $\eta < 1.55$ & $q > 0.8$	Low η - low q $\eta < 1.55$ & $q < 0.55$
$\langle\eta\rangle$	10.40	-8.59	-9.79
$\langle q\rangle$	31.51	27.80	-43.18
$\langle LSI\rangle$	81.74	-56.61	-46.87
$\langle S_k\rangle$	0.04	-0.02	-0.05
$\langle n_{coor,3.7A^\circ}\rangle$	-13.9	16.8	11.0

We repeated the same analysis for the η and LSI parameters. While η and LSI are both directly sensitive to interstitial water molecules beyond the first shell, low LSI values are found for structures with a broad range of η values (Fig. 1). Table S2 shows that in (high η, low LSI) structures, the coordination number within 3.7 Å is large. This suggests that the LSI is more sensitive than η to the presence of interstitial water molecules and to a crowded second shell beyond the first shell. It can be readily seen from the definition of the LSI Eq. 3 that for two concentric spherical shells within 3.7 Å, an increase in the coordination

number implies a decrease in the LSI value. The LSI is thus not only sensitive to the local tetrahedral arrangement but also to the local density in the second shell. In contrast, the asphericity η does not depend on any arbitrary cut-off distance and is not sensitive to the second-shell density. (high η, low LSI) structures thus correspond to arrangements where the first shell is tetrahedral but where the second-shell is nearby.

Table S2: Average relative shifts in η, q, LSI and S_k with respect to their 298 K bulk averages (in %) for all water neighbors within 3.7 Å and for a series of different configuration subensembles defined by the range of η and LSI values.

	$\eta > 1.75$ & $LSI > 0.05$	$\eta > 1.75$ & $LSI < 0.05$	$\eta < 1.55$ & $LSI < 0.05$
η	10.60	7.97	-9.63
q	18.73	15.18	-23.45
LSI	167.78	-71.23	-76.20
S_k	0.05	-0.01	-0.01
$n_{coor,3.7\mathring{A}}$	-19.7	2.9	20.5

Influence of transformation from TIP4P/2005 to SPC/E geometries for electric field calculations. As explained in the methodology section of the main text, for electric field calculations, the geometry and charges of each TIP4P/2005 water molecule is turned into a SPC/E water molecule, in order to connect the computed electric field to a vibrational frequency through an empirical frequency map, which is available only for SPC/E water. Fig. S2 compares the resulting electric field distributions in the bulk and in the shell at 298 K for both models. While the change of geometry alters significantly the width and mean of the distributions, a major point for our study is that the difference between bulk and shell distributions is very similar in both descriptions. Moreover, the Pearson correlation coefficient between the two calculations of the electric field is 0.978, which shows that the two values of the electric field before and after the geometrical transformation are very well correlated.

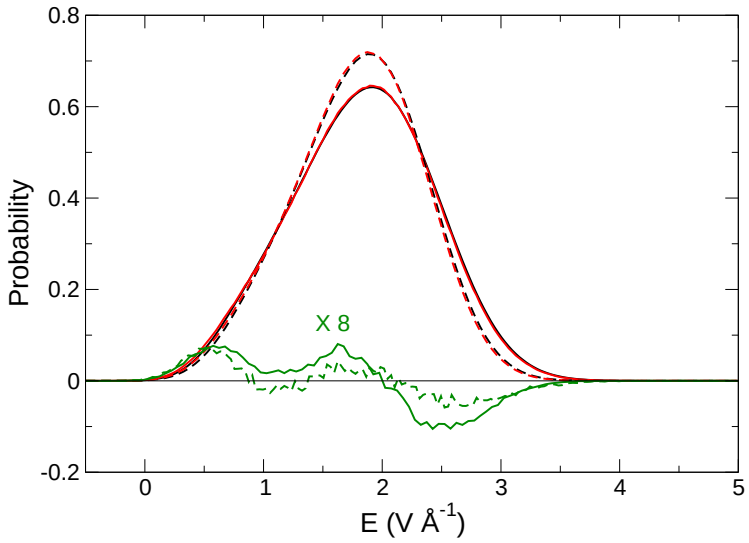

Figure S2: Electric field distribution in the bulk (black) and in the shell (red), together with their difference (green), with the initial TIP4P/2005 geometry, and after its transformation to the SPC/E water model.

Complementary analysis of the structural change induced by a decrease in temperature

Figure S3 shows the distributions of water local structures as measured by S_k in the bulk at 298 K and at 260 K to complement Fig. 2 in the main text.

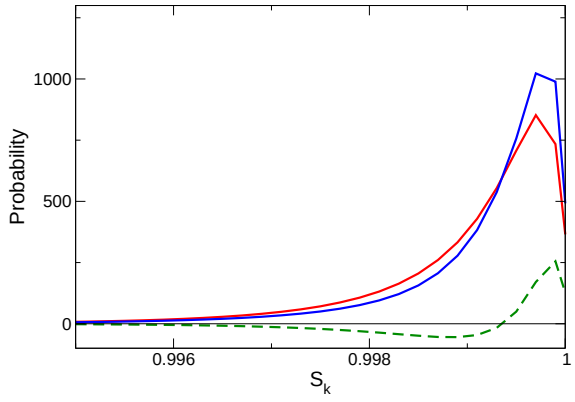

Figure S3: S_k probability distributions in bulk water at 298 K (red) and at 260 K (blue) together with their difference (green).

Complementary structural analysis of the hydrophobic hydration shell

The S_k, E and ρ distributions respectively in the bulk and in the hydrophobic part of the shell of propanol at 298 K are shown in Fig.S4, in complement of Fig. 3. Table S3 shows that the Pearson correlation coefficients between order parameters for water molecules in shell display the same behavior as the correlations determined in the bulk and presented in Table 1.

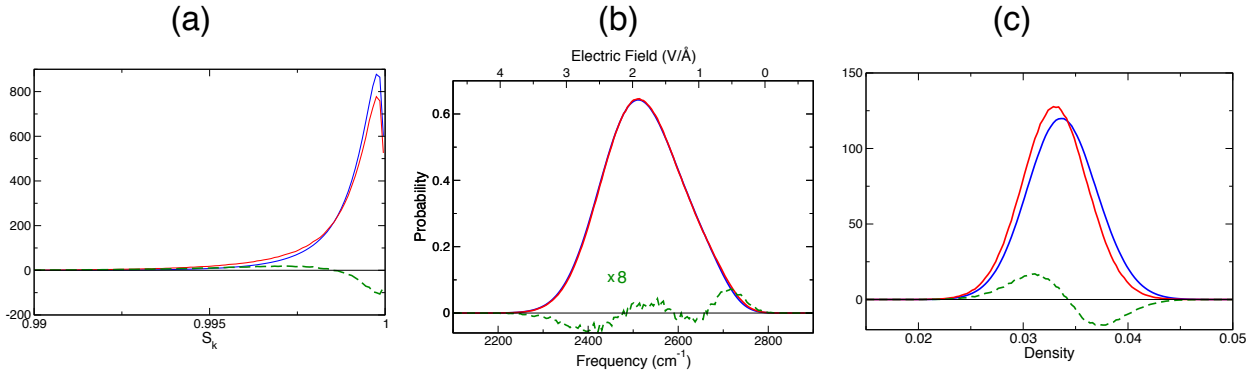

Figure S4: Distribution of the order parameters S_k, E and ρ respectively in bulk water and in the hydrophobic part of the hydration shell at 298 K together with their difference (dashed green).

Table S3: Pearson correlation coefficient for water molecules in the hydrophobic part of the hydration shell at 298 K.

	Asphericity	Density	q	S_k	LSI	E
Asphericity	1.0	0.07	0.51	0.21	0.48	0.40
Density	0.07	1.0	0.23	0.41	-0.14	0.31
q	0.51	0.23	1.0	0.37	0.16	0.31
S_k	0.21	0.41	0.37	1.0	0.002	0.18
LSI	0.48	-0.14	0.16	0.002	1.0	0.23
E	0.40	0.31	0.31	0.18	0.23	1.0

The comparison of the average structural parameter values in the shell and in the bulk at 260 K provided in Table S4 exhibits the same features as at 300 K, which are discussed in the main text.

Table S4: Mean values of order parameters for water molecules lying respectively in the bulk and in the hydrophobic part of the n-propanol hydration shell at 260 K, together with the relative change from bulk to shell.

	bulk	shell	relative change (%)
Asphericity	1.7048	1.7051	0.01
Density (Å^{-3})	0.03364	0.03318	-1.38
q	0.7297	0.7154	-1.96
S_k	0.9992	0.9989	-0.02
LSI (Å^2)	0.0509	0.0707	38.83
E ($V\text{Å}^{-1}$)	1.9648	1.9655	0.03

Structural fluctuations affecting water reorientation dynamics.

Table S5 gives the reorientation times for water molecules initially lying in the hydrophobic hydration shell and with different initial values of the structural order parameters. The conclusions are similar to these in the bulk (Table 4) and show that the asphericity is again found to capture best the structural fluctuations that affect water reorientation dynamics. The presence of the hydrophobic solute therefore does not change the conclusion, and suggests that potential solute-induced artifacts are very limited.

Table S5: Integrated OH reorientation times τ_{reor} Eq. 8 of shell water molecules at 298 K whose initial order parameter value respectively lies in the first (Q1), second and third (Q2-Q3) and fourth (Q4) quartiles of the order parameter distribution.

	Q1	Q2-Q3	Q4
Asphericity	2.10	2.85	3.48
Density	2.69	2.91	2.79
q	2.21	2.85	3.48
S_k	2.49	2.84	3.12
LSI	2.39	2.82	3.37
E	2.15	2.98	3.28

Solute artefacts in asphericity calculation

The Voronoi cell includes all points that are closer to the central water oxygen than to any other heavy atom, including solute atoms. Thus, the asphericity of the cell next to a hydrophobic solute is partly determined by the solute interface, and does not exclusively

reflect the structure of water. However, the potential artifact in η is expected to be small, since the Voronoi cell is mainly determined by the four nearest neighbors which are all water molecules. This is confirmed by our calculation of the fraction of the Voronoi cell surface that is in contact with the solute (Fig. S5). This fraction is shown to be always small (<11%) and to decrease for increasing η. Therefore, the more ordered the local structure, the lower the fraction of the surface in contact with the solute, the smaller the artefact due to the solute interface. The artifact in η due to the solute presence is therefore very limited, but its effect on the η value is difficult to remove.

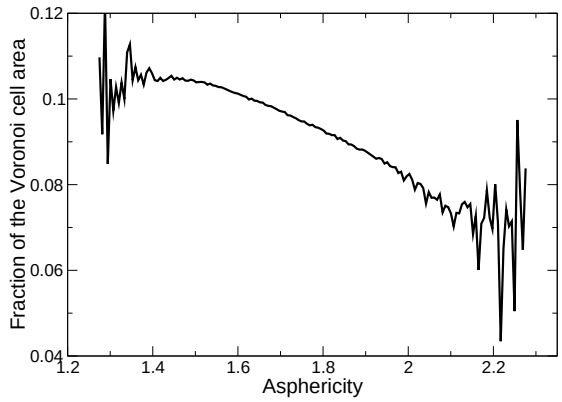

Figure S5: Average fraction of a shell water molecule Voronoi cell in contact with the solute for different values of the Voronoi asphericity.

On the use of the H-bond angle to probe the water local structure.

The distribution $P(\theta)$, where θ stands for the smallest H-O–O angle between a pair of water molecules, has been used to characterize the water local structure, e.g. in the bulk[1] and next to solutes, including hydrophobic solutes[2] and proteins.[3,4] This distribution usually exhibits two peaks, respectively at smaller and larger θ values. However, our calculations confirm prior studies[5] and show that the population in the second peak is very sensitive to the chosen cut-off radius for the pairs of water molecules (Fig. S6a). While the second peak has sometimes been assigned to distorted hydrogen-bonds, it appears that it rather arises

from two water molecules which are normally hydrogen-bonded to their respective neighbors but which are located in the second shell of each other.

What is represented is often a probability density, and the underlying probability is thus $P(\theta)/\sin(\theta)$. The results in Fig. S6b display the expected peak for linear hydrogen-bonds and the width of the peak is a measure of the size of the librational cone in which the OH bond wobbles, and is thus a probe of the hydrogen-bond strength. Similar analyses have for example been presented for water-anion hydrogen-bonds.[6]

The comparison of the $P(\theta)$ distributions at 300 K and 260 K confirms the expected increase in hydrogen-bond strength and the enhancement of the peak at small θ values.

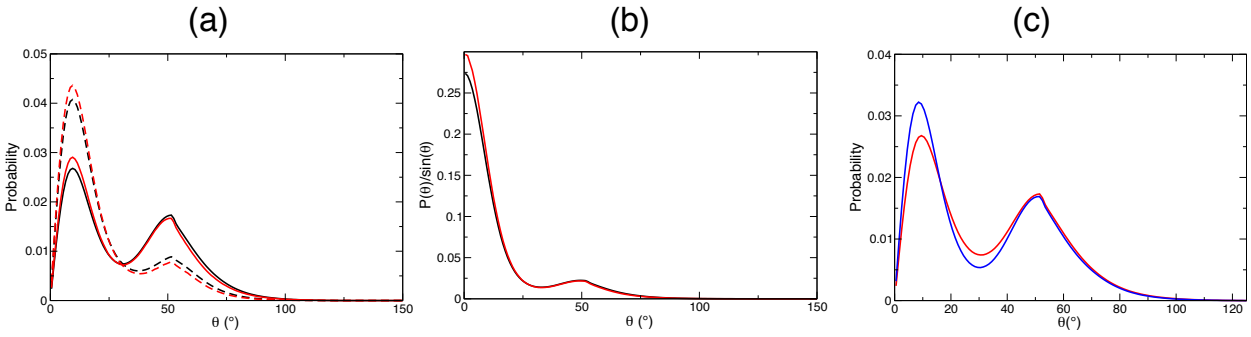

Figure S6: (A) Distributions of H-OH angles between pairs of water molecules at 298 K depending on the initial location of the water molecule : in the bulk (back) and in the shell (red). The calculation is made using two different cutoff values used in the literature, 3.5 (dashed lines) and 4.0 Å (plain lines) (b) Bulk and shell $\frac{p(\theta)}{\sin(\theta)}$ distributions with a 4.0 Å cutoff at 298 K. (C) Comparaison of θ distributions in the bulk at 298 K (red) and 260 K. (blue)

References

(1) Madan, B.; Sharp, K. Heat Capacity Changes Accompanying Hydrophobic and Ionic Solvation: a Monte Carlo and Random Network Model Study. *J. Phys. Chem.* **1996**, *100*, 7713–7721.

(2) Sharp, K. A.; Madan, B. Hydrophobic Effect, Water Structure, and Heat Capacity Changes. *J. Phys. Chem. B* **1997**, *101*, 4343–4348.

(3) Yang, C.; Sharp, K. A. The Mechanism of the Type III Antifreeze Protein Action: a Computational Study. *Biophys. Chem.* **2004**, *109*, 137–148.

(4) Yang, C.; Sharp, K. A. Hydrophobic Tendency of Polar Group Hydration as a Major Force in Type I Antifreeze Protein Recognition. *Proteins: Struct., Funct., Bioinf.* **2005**, *59*, 266–274.

(5) Sharp, K. A.; Vanderkooi, J. M. Water in the Half Shell: Structure of Water, Focusing on Angular Structure and Solvation. *Acc. Chem. Res.* **2010**, *43*, 231–239.

(6) Stirnemann, G.; Wernersson, E.; Jungwirth, P.; Laage, D. Mechanisms of Acceleration and Retardation of Water Dynamics by Ions. *J Am Chem Soc* **2013**, *135*, 11824–11831.